

CONTENTS

	Page
Acknowledgement	d
Abstract in Thai	g
Abstract in English	i
List of Tables	o
List of Figures	q
Statement of Originality in Thai	v
Statement of Originality in English	w
Chapter 1 Introduction	1
Chapter 2 Literature Survey	4
2.1 Classification of Stainless Steels and Effects of Alloying Elements on Their Structure and Properties	4
2.2 The Mn-substituted Austenitic Stainless Steels	12
2.3 Welding Process for Thin Plate Austenitic Stainless Steels	13
2.3.1 Pulsed Current TIG Arc Welding or Pulsed Gas Tungsten Arc Welding for Thin Plate without Filler	16
2.3.2 Effect of Welding Parameters on TIGW/GTAW for Thin Plate Welding without Filler	17
- Cooling rate	17
- Shielding gas	17
2.4 Solidification of Weld Fusion Zones in Austenitic and Weldments	19
2.4.1 Phase Transformation During Cooling Cycle of the Weld Metals	19

2.4.2 Microstructure and Solidification Mode in Welded Austenitic Stainless Steels	19
2.4.2.1 Microstructure Classification by Cr- and Ni-Equivalency Ratio	19
2.4.2.2 Primary Solidification Modes in Welded Austenitic Stainless Steels	21
2.5 Corrosion of Stainless Steels and Weldment	27
2.6 Micro-Vickers Hardness (MVH) of Weldment	32
2.7 Tensile Properties of Weldment	33
Chapter 3 Experimental Procedures	35
3.1 Objectives	35
3.2 Materials and Summary of Methodology	35
3.3 Pulsed Current Tungsten Inert Gas Welding (PCTIGW)	36
3.4 Chemical Analysis of Base Metals by Glow Discharge Spectrometry (GDS)	40
3.5 Chemical Analysis of Weldment by Oxygen/ Nitrogen Combustion Analysis	42
3.6 Phase Identification by X-ray Diffractometry and Ferritescope	42
3.7 Microstructural Investigation by Optical Microscopy	44
3.8 Microstructural Investigation by Scanning Electron Microscopy and Electron Probe Microanalysis	45
3.9 Pitting Corrosion Resistance Test	46
3.10 Degree of Sensitization Test	48
3.11 Micro-Vicker Hardness Test of Weldment	49
3.12 Tensile Test	50
Chapter 4 Results and Discussion	52
4.1 Chemical Analysis and Phase Identification of Base ASSs	52
4.2 Pitting Corrosion Resistance of Base ASSs	56
4.3 Intergranular Corrosion Susceptibility of Base ASSs	61
4.4 Mechanical Properties of Base ASSs	66

4.4.1 Tensile Properties	66
4.4.2 Micro-Vickers Hardness Test	66
4.5 Prediction of Structure Type and Solidification Mode and Weldments	68
4.6 Dissolved Nitrogen in Weld Pool and Ferrite Content	69
4.7 Weld Pool Inspection	76
4.8 Pitting Corrosion Resistance (PCR) of Weldment	81
4.8.1 PCGTAW AISI 304	85
4.8.2 PCGTAW AISI 304L	87
4.8.3 PCGTAW 201-2M	89
4.8.4 PCGTAW AISI 202	91
4.9 Degree of Sensitization of Weldment	94
4.9.1 PCGTAW AISI 304	94
4.9.2 PCGTAW AISI 304L	98
4.9.3 PCGTAW 201-2M	101
4.9.4 PCGTAW AISI 202	104
4.10 Tensile Properties of Weldment	108
4.11 Micro-Vickers Hardness of Weldment	111
 Chapter 5 Conclusions and Further Work	 115
5.1 Base Metals	115
5.1.1 Chemical Composition	115
5.1.2 Corrosion Resistance Properties	115
5.1.3 Mechanical Properties	116
5.2 PCGTAW Austenitic Stainless Steels	116
5.2.1 Welding Process Control Parameters	116
5.2.2 Weld Structure Prediction	116
5.2.3 Pitting Corrosion Resistance	116
5.2.4 Degree of Sensitization	117
5.2.5 Mechanical Properties	117
5.3 Future Work	117
 References	 118

Appendices

Appendix A	Different in Temperature Gradients Tables	138
Appendix B	Weld Pool Inspection Tables	140
Appendix C	Tensile Properties Tables	143
Appendix D	Autolab GPES Version 4.9: Corrosion Rate Calculation	145

Curriculum Vitae		148
------------------	--	-----

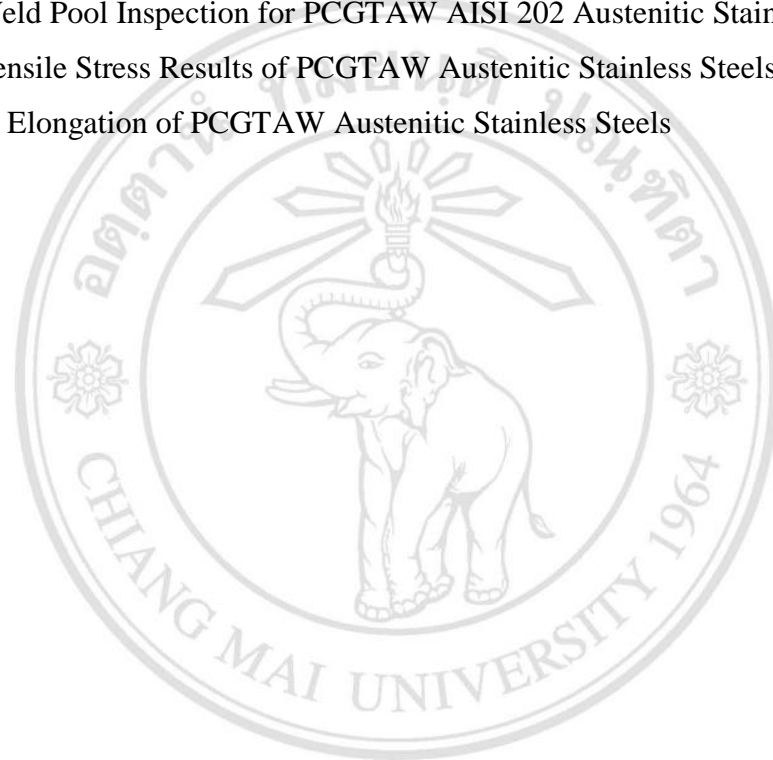


ลิขสิทธิ์มหาวิทยาลัยเชียงใหม่
Copyright© by Chiang Mai University
All rights reserved

LIST OF TABLES

	Page
Table 2.1 Classification of Stainless Steels by Dominant Microstructure	6
Table 2.2 Summary of Modified Equivalencies Cr and Ni Calculation	10
Table 2.3 Stacking Fault Energy Estimation for Austenitic Stainless Steels	12
Table 2.4 Notations	22
Table 2.5 Solidification Mode, Solidification Sequence, and Solid-state Transformation Responsible for the Variation in Fusion Zone Of Welds Austenitic Stainless Steels	23
Table 3.1 Experimental Austenitic Stainless Steels	35
Table 3.2 Summary of Methology	36
Table 3.3 Controlled Parameters	37
Table 3.4 Variable Parameters	37
Table 3.5 Calculated Heat Input at Various Welding Current and N ₂ Percentage in Shielding Gas	38
Table 4.1 Chemical Analysis of Base ASSs by GDS	53
Table 4.2 UNS Chemical Composition of ASSs	53
Table 4.3 Calculated Parameters of Base ASSs	54
Table 4.4 $PREN_{Mn}$ and Pit Depth in Base ASSs	57
Table 4.5 Corrosion Parameters of Base ASSs	59
Table 4.6 DOS Test of Base ASSs	61
Table 4.7 Tensile Properties	66
Table 4.8 Micro-Vickers Hardness (MVH) of Base ASSs	66
Table 4.9 Calculated Parameters of Austenitic Stainless Steels	68
Table 4.10 Average Weld Metal Nitrogen Contents in Different Weld Samples	70
Table 4.11 Ferrite Contents as δ -ferrite and FN in ASS Weldment	71
Table 4.12 Calculation on Pitting Corrosion Resistance at I = 130A	81
Table 4.13 Calculation on Pitting Corrosion Resistance at I = 160A	82
Table 4.14 DOS of PCGTAW AISI 304Stainless Steels	97
Table 4.15 DOS of PCGTAW AISI 304L Austenitic Stainless Steels	100
Table 4.16 DOS of PCGTAW 201-2M Austenitic Stainless Steels	103

Table 4.17	DOS of PCGTAW AISI 202 Austenitic Stainless Steels	106
Table A1	Peak Temperature at Position 1 to 5. Welding Current 130 Amp	138
Table A2	Peak Temperature at Position 1 to 5. Welding Current 160 Amp	139
Table B1	Weld Pool Inspection for PCGTAW AISI 304 Austenitic Stainless Steels	140
Table B2	Weld Pool Inspection for PCGTAW AISI 304L Austenitic Stainless Steels	141
Table B3	Weld Pool Inspection for PCGTAW 201-2M Austenitic Stainless Steels	141
Table B4	Weld Pool Inspection for PCGTAW AISI 202 Austenitic Stainless Steels	142
Table C1	Tensile Stress Results of PCGTAW Austenitic Stainless Steels	143
Table C2	% Elongation of PCGTAW Austenitic Stainless Steels	144



ลิขสิทธิ์มหาวิทยาลัยเชียงใหม่
 Copyright© by Chiang Mai University
 All rights reserved

LIST OF FIGURES

	Page
Figure 2.1 Illustration of Fe-Cr Phase Diagram	4
Figure 2.2 Fe-Cr Phase diagram from Brystan's work	11
Figure 2.3 Schematic illustration of typical TIG/GTAW process	14
Figure 2.4 Regions of a fusion weld	15
Figure 2.5 Illustrations of isotherms about the heat sources in fusion welding, the shape of weld beads, the weld pool shape and penetration	15
Figure 2.6 Illustrations of tear drop and elliptical bead front	16
Figure 2.7 Morphology of vermicular and lacy (lathy) ferrite in weld Microstructure of austenitic stainless steels	20
Figure 2.8 Microstructure types and the amount of δ -ferrite in structure of welded austenitic stainless steels as predicted by the Schaeffler diagram	21
Figure 2.9 Solidification mode in fusion zone of welds austenitic stainless steels	26
Figure 2.10 Potential stages during passive film break down and pitting is occurred	28
Figure 2.11 Illustration of pitting corrosion forming at deteriorated sites sites in protective film of stainless steels	29
Figure 2.12 Double loop electrochemical potentiodynamic reactivation (DL-EPR) methodology according to ASTM G108 for determining degree of sensitization (DOS) in ASSs	30
Figure 2.13 DL-EPR loop shapes	31
Figure 2.14 Classification of sensitized microstructure according to ASTM A262-2008	31
Figure 2.15 Illustration of micro-Vickers indenter layout and mean diagonal measurement following ASTM E384 standard practice	33
Figure 3.1 The work bench and the array of welding torch and shielding gas nozzles	38
Figure 3.2 Schematic drawing showing five positions of thermocouples attached to the weld plate	39
Figure 3.3 Inner chamber of glow discharge spectrometer (LECO GDS 850A) where sample was attached	40

Figure 3.4	Mechanism of glow discharge spectroscopy (GDS)	41
Figure 3.5	Oxygen/ Nitrogen Analyzer, Horiba EMGA -920	42
Figure 3.6	Rikaku TTRAXIII X-ray diffractometer	43
Figure 3.7	Ferritescope, Fischer GmbH FMP 30	44
Figure 3.8	The line-intercept method per instruction in ASTM E112-08	44
Figure 3.9	Shimadzu-1610 EPMA	45
Figure 3.10	Three electrode cell for pitting corrosion resistance test: flat cell	46
Figure 3.11	Pit morphology observation in terms of width, depth and volume density in according to ASTM G108 for detecting sensitization in ASSs	47
Figure 3.12(a)	Vickers indenter, (b) Anton Paar, PaarPhysica, MHT-10micro-hardness tester	49
Figure 3.13	Illustration of dog bone specimens for tensile test	51
Figure 4.1	Prediction plots in Schaeffler diagram from the chemical composition Of base ASSs	54
Figure 4.2	Phase identification by XRD of base ASSs	55
Figure 4.3	Morphology of pits in (a) AISI 304 and (b) 201-2M after performed pitting resistance corrosion test by means of cyclic potentiodynamic polarization technique	56
Figure 4.4	Cyclic potentiodynamic polarization curves of base ASSs	58
Figure 4.5	A trend between corrosion potential (E_{corr}) and pitting potential (E_p) Of base ASSs	60
Figure 4.6	DOS test results of AISI 304 austenitic stainless steel: a) microstructure of original grain orientation in the normal direction to the cold-rolling direction ($G = 16.94$), (b) DL-EPR curve and (c) sensitized microstructure	62
Figure 4.7	DOS test results of 201-2M austenitic stainless steel: a) microstructure of original grain orientation in the normal direction to the cold-rolling direction ($G = 16.94$), (b) DL-EPR curve and (c) sensitized microstructure	63
Figure 4.8	DOS test results of AISI 202 austenitic stainless steel: a) microstructure of original grain orientation in the normal direction to the cold-rolling direction ($G = 16.94$), (b) DL-EPR curve and	64

	(c) sensitized microstructure	
Figure 4.9	(a) Detected weight percentage of nitrogen and (b) FN in weld metal of AISI 304 at different mixed ratio of N ₂ : Ar shielding gas at welding current 130 and 160 A	72
Figure 4.10	(a) Detected weight percentage of nitrogen and (b) FN in weld metal of AISI 304Lat different mixed ratio of N ₂ : Ar shielding gas at welding current 130 and 160 A	73
Figure 4.11	(a) Detected weight percentage of nitrogen and (b) FN in weld metal of 201-2Mat different mixed ratio of N ₂ : Ar shielding gas at welding current 130 and 160 A	74
Figure 4.12	(a) Detected weight percentage of nitrogen and (b) FN in weld metal of AISI 202at different mixed ratio of N ₂ : Arshielding gas at welding current 130 and 160 A	75
Figure 4.13	(a), (b) Weld pool inspection of PCGTAW AISI 304, shielding gas ratio = 0N ₂ :100Ar, (c) weld pool front width and (d) completed penetration depth, at welding current 130 and 160 Amp, respectively	77
Figure 4.14	(a), (b) Weld pool inspection of PCGTAW AISI 304L, shielding gas ratio = 0N ₂ :100Ar and 5:95, (c) weld pool front width and (d) completed penetration depth, at welding current 130 and 160 Amp, respectively	78
Figure 4.15	(a), (b) Weld pool inspection of PCGTAW 201-2M, shielding gas ratio = 5:95, (c) weld pool front width and (d) completed penetration depth at welding current 130 and 160 A, respectively	79
Figure 4.16	(a), (b) Weld pool inspection of PCGTAW AISI 202, shielding gas ratio = 5:95, (c) weld pool front width and (d) completed penetration depth at welding current 130 and 160 A, respectively	80
Figure 4.17	(a) and (b) pit depth in the observed area across weld specimen with change in pitting potentials at different welding currents and under various mixed shielding gases, (c) and (d) pit density distribution in the observed area across weld specimen with change in pitting potentials at different welding currents and under various mixed shielding gases.	83

Figure 4.18 Pit morphology of PCGTAW AISI 304	85
Figure 4.19 CV potentiodynamic polarization curves of PCGTAW AISI 304 at welding current 130 and 160 A under various ratio of N ₂ :Ar shielding gases	86
Figure 4.20 Pit morphology of PCGTAW AISI 304	87
Figure 4.21 CV potentiodynamic polarization curves of PCGTAW AISI 304L at welding current 130 and 160 A under various ratio of N ₂ :Ar shielding gases	88
Figure 4.22 Pit morphology of PCGTAW AISI 304	89
Figure 4.23 CV potentiodynamic polarization curves of PCGTAW 201-2M at current 130 and 160 A under various ratio of Ar:N ₂ shielding gases	90
Figure 4.24 Pit morphology of PCGTAW AISI 202	91
Figure 4.25 CV potentiodynamic polarization curves of PCGTAW AISI 202 at welding current 130 and 160 A under various ratio of Ar:N ₂ shielding gases	92
Figure 4.26 Grain boundary morphology of sensitized PCGTAW AISI 304 and DLEPR plots at welding current 130 and 160 A under 5N ₂ :95 Ar	96
Figure 4.27 Grain boundary morphology of sensitized PCGTAW AISI 304L and DLEPR plots at welding current 130 and 160 A under current 130 and 160 Amp under 5N ₂ :95 Ar	99
Figure 4.28 Grain boundary morphology of sensitized PCGTAW 201-2M and DLEPR plots at welding current 130 and 160 A under current 130 and 160 Amp under 10N ₂ :90 Ar	100
Figure 4.29 Grain boundary morphology of sensitized PCGTAW AISI 202 and DLEPR plots at welding current 130 and 160 A under current 130 and 160 Amp under 10N ₂ :90 Ar	103
Figure 4.30 Change in DOS under different N ₂ proportion in shielding gas and welding current at 130 and 160 A current 130 and 160 Amp under 10N ₂ :90 Ar	107
Figure 4.31 Comparison of tensile strength of PCGTAW austenitic stainless steels at welding current 130 and 160 A under 0, 5 and	109

10 vol.%N ₂ shielding gases	
Figure 4.32 Comparison of % elongation of PCGTAW austenitic stainless steels under various vol.% nitrogen (0, 5 and 10 %) in shielding gases	109
Figure 4.33 Examples of fracture surface of the base metals and PCGTAW weldment at welding current 130 and 160 A under Ar:N ₂ = 95:5	110
Figure 4.34 MVH of weld cross-section of PCGTAW AISI 304 at welding current 130 and 160 A	111
Figure 4.35 MVH of weld cross-section of PCGTAW AISI 304Lat welding current 130 and 160 A	111
Figure 4.36 MVH of weld cross-section of PCGTAW 201-2Mat welding current 130 and 160 A	112
Figure 4.37 MVH of weld cross-section of PCGTAW AISI 202at welding current 130 and 160 A	112
Figure ANNEX D.1 Tafel plot generated in Corrosion rate analysis Windows by Autolab GPES Ver.4.9	147

ข้อความแห่งการริเริ่ม

- 1) ความริเริ่มในเชิงทฤษฎี การศึกษาโครงสร้างทางจุลภาคของการเปลี่ยนเฟส และการสร้างเฟสใหม่ตรงบริเวณขอบเขตระหว่างโลหะดั้งเดิม สิทอเฟเฟลท์โซน และบริเวณโลหะหลอมเหลว ในงานเชื่อมแบบทิก ของแผ่นเหล็กกล้าไร้สนิมออสติเนติก เกรดเอไอเอสไอ 304 และเกรดที่มีการแทนที่บางส่วนด้วยแมงกานีส หรือเกรด 200 โดยใช้กล้องจุลทรรศน์แบบแสง และกล้องจุลทรรศน์อิเล็กตรอน จะช่วยให้เกิดองค์ความรู้ใหม่เผยแพร่สู่ระดับสากล ในด้านที่เกี่ยวกับสมบัติโลหะทางกายภาพของงานเชื่อมโลหะ
- 2) ความริเริ่มในเชิงปฏิบัติ ความเข้าใจในความสัมพันธ์ระหว่างโครงสร้างและสมบัติ ของงานเชื่อมแบบทิกของเหล็กกล้าไร้สนิม จะช่วยให้มีความเผยแพร่ความรู้ และรายละเอียดเพิ่มเติม เพื่อการประยุกต์ใช้งานจริงทางภาคอุตสาหกรรม และบ่งชี้ตัวควบคุมที่มีความสำคัญในกระบวนการเชื่อมโลหะ นอกจากนี้ เมื่อคำนึงถึงต้นทุนการประยุกต์ใช้งานทางด้านอุตสาหกรรมต่อแล้ว ในสภาพแวดล้อมที่มีความกัดกร่อนน้อย มีความเป็นไปได้ ในการนำเหล็กกล้าไร้สนิมเกรด 200 มาเป็นตัวเลือกทดแทนการใช้งานเหล็กกล้าไร้สนิมเกรดเอไอเอสไอ 304

ลิขสิทธิ์มหาวิทยาลัยเชียงใหม่
Copyright© by Chiang Mai University
All rights reserved

STATEMENTS OF ORIGINALITY

- 1) Theoretically, the novel observation on microstructure of phase transformation and re-forming at the boundary among base metal, heat affected zone (HAZ) and fusion area of the TIG welded Mn-substitution austenitic stainless steels and reference AISI 304 mainly obtained by means of optical and electron microscopy will lead to an international contribution on the knowledge of physical metallurgy of welding.
- 2) Practically, the understanding of structure and property relationship of TIG welded stainless steels will contribute to/in details for industrial applications and indicate crucial controlled parameters in welding process. Regarding the cost effective reason in pipeline application, the Mn-substitution austenitic stainless steel may possible to introduce for the utilization in mild corrosive environment as an alternative to AISI 304.

ลิขสิทธิ์มหาวิทยาลัยเชียงใหม่
Copyright© by Chiang Mai University
All rights reserved